

Structures and Proton Conductivity of One-Dimensional M(dhbq)·nH$_2$O (M = Mg, Mn, Co, Ni, and Zn, H$_2$(dhbq) = 2,5-Dihydroxy-1,4-benzoquinone) Promoted by Connected Hydrogen-Bond Networks with Absorbed Water

Teppei Yamada,[*1] **Shota Morikawa,**[1] **and Hiroshi Kitagawa**[*1,2,3]

[1]Department of Chemistry, Faculty of Science, Kyushu University, 6-10-1 Hakozaki, Higashi-ku, Fukuoka 812-8581

[2]Department of Chemistry, Graduate School of Science, Kyoto University, Kitashirakawa-Oiwakecho, Sakyo-ku, Kyoto 606-8502

[3]JST CREST, 5 Sanbancho, Chiyoda-ku, Tokyo 102-0075

Received August 18, 2009; E-mail: teppei343@gmail.com

One-dimensional (1D) coordination polymers, M(dhbq)·nH$_2$O (M = Mg, Mn, Co, Ni, and Zn, H$_2$(dhbq) = 2,5-dihydroxy-1,4-benzoquinone, n = 2, 2.5, or 3), were synthesized and their structures were investigated using the Rietveld refinement method. They have 1D structure and were isostructural. From water uptake measurements, thermogravimetry, and elemental analysis, new 2.5 hydrate states were discovered. The proton conductivity of M(dhbq) was found to depend on the metal species and the quantity of absorbed water.

Much attention has been focused on coordination polymers (CPs) or metal–organic frameworks over decades[1] because they have high degrees of freedom in metal ions and bridging ligands to construct highly ordered structures. They have been reported to show high specific surface area, high capacity for gas storage,[2] or catalytic activity,[3] because of an anomalous interaction between the guest molecules and the inner surface of the frameworks of the CPs. One-dimensional (1D) or two-dimensional CPs have also been synthesized and reported by choosing ligands and the coordination geometry of the metal sites.[4] They contain highly ordered interfaces at interchains or interlayers; the nanoscale interfaces offer constrained spaces and can affect the interaction with the guest molecules in the nanospace.

The dynamics of guest molecules in restrained spaces or interfaces are also thought to be different from those of bulk materials. In particular, the proton conductivity of interfacial space has been intensively studied since the proton conductivity of $MHSO_4$ (M = K, Cs, and Rb) was enhanced by mixing heterogeneously with highly dispersed silica at ambient temperature.[5] Maier and co-workers reported that the proton conductivity of liquid imidazole is enhanced when it is mixed heterogeneously with TiO_2, Al_2O_3, or ZrO_2.[6] They concluded that the enhancement resulted from the formation of a space-charge layer at the interfaces. The reason for the conductivity improvement is still under discussion, but an interface of nanoscale thickness is thought to be related to the conductivity.

To study the proton dynamics of CPs, functionalized CPs have been synthesized in sophisticated ways.[7] The proton conductivity of several CPs was investigated, and those consisting of dithiooxamide and its derivatives showed high proton conductivity when water molecules were introduced into the pores under humidified conditions.[8] The proton conductivity of iron(II) oxalate dihydrate was also evaluated and found to be high.[9] The proton carrier of the conventional proton conductor originates from strong acidic functional groups such as sulfonic acid; however, the carrier for iron(II) oxalate dihydrate was the coordination water molecules. The high proton conductivity was thought to be derived from the 1D array of water chains in the nanoscale interfaces of the 1D chains of iron(II) oxalate dihydrate however much study was required to elucidate the proton conduction mechanisms.

CPs of dhbq (H$_2$(dhbq) = 2,5-dihydroxy-1,4-benzoquinone) were reported at an early time by the groups of Kanda, Miyoshi, and Rao, and assumed to form 1D alternate chains of metal ions and bridging ligands.[10–13] However, to our knowledge, there have been no reports of the crystal structure of metal–dhbq compounds since we succeeded in determining the crystal structure of Mn(dhbq)·2H$_2$O by single-crystal X-ray diffraction analysis (Figure 1).[14] Its proton conductivity was also studied and was found to reach 10^{-4} S cm^{-1} at ambient temperature. Thus, the proton conducting mechanism of 1D CPs has become an active topic.

To study the proton dynamics of the water array in the nanospace of the interchain, we prepared a series of 1D metal–dhbq compounds. X-ray powder diffraction (XRPD) patterns of them were collected and their structures were determined using the Rietveld refinement method. Water absorption isotherms and proton conductivity under various humidity conditions were also measured, and proton conduction mechanisms of these compounds are discussed.

Results and Discussion

Synthesis. M(dhbq)·nH$_2$O (M = Mg, Mn, Co, Ni, and Zn) was synthesized according to the scheme shown in Figure 2.

Published on the web December 23, 2009; doi:10.1246/bcsj.20090216

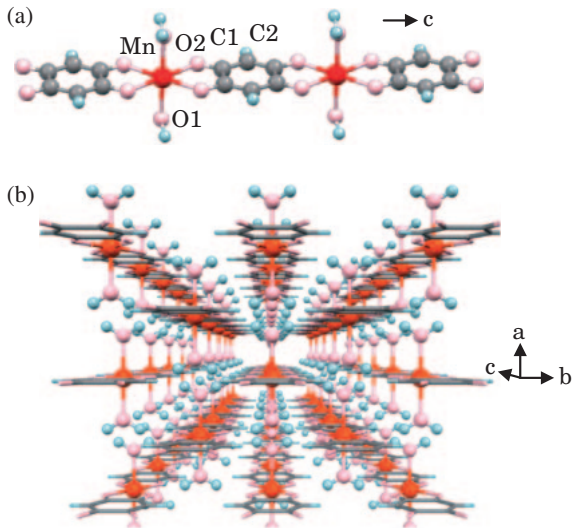

Figure 1. Crystal structure of (a) 1D arrangement and (b) perspective view along the *b* axis of Mn(dhbq)·2H_2O. Red (a) or orange (b), pink, gray, and blue balls correspond to manganese, oxygen, carbon, and hydrogen atoms, respectively.[10]

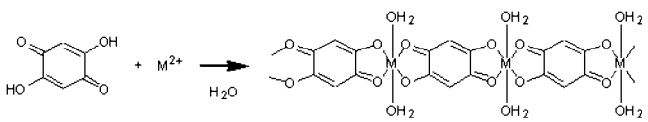

Figure 2. Synthesis scheme for M(dhbq)·$n$$H_2O$.

Results of elemental analyses (EA) for Mg and Zn compounds are in good agreement with the calculated values for the dihydrate state. In contrast, EA results of the other CPs cannot be fitted to the calculated values for dihydrates. The analysis of Co and Mg compounds can be fitted to those of 2.5 hydrates, and the Ni compound contains three water molecules.

1D CPs of M(ox) (M = Mg, Mn, Co, and Zn) were reported to contain two water per each metal site, independent of metal species. There are few papers reporting the syntheses and identification of 1D dhbq compounds, and their water content depends on the synthesis conditions. Miyoshi and co-workers reported that the Ni compound contained three equivalents of water when it was synthesized in ethanol solution.[10] Bottei and Fangman reported the EA of Co, Ni, Cu, and Zn compounds, and their results can be best fitted to 2.2, 3.0, 2.5, and 2.3 equivalents of water molecules, respectively.[11] Talati and Mistry succeeded in synthesizing Co(dhbq)·2H_2O using ethanol as a solvent.[12] We therefore conducted thermogravimetric (TG) analyses and water uptake measurements.

Structures. The crystal structure of Mn(dhbq)·2H_2O contains a void, and residual electron density peaks were observed at the void (Figure 3). Distances from the oxygen atoms of water molecules to a residual electron density peak were 2.71 and 3.64 Å, respectively, which are comparable with the hydrogen-bond distance. Two positions of residual electron density peaks were observed at one equivalent of Mn(dhbq)·2H_2O. From these results, Mn(dhbq) contains two water molecules coordinating to the metal site at ambient humidity, and the compound has the potential to absorb more water molecules into

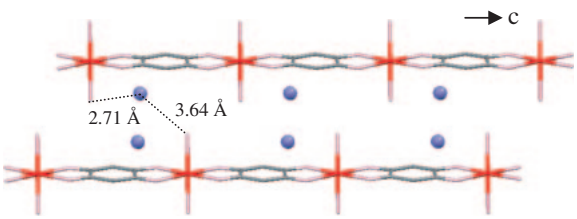

Figure 3. Crystal structure and residual peaks of electron density (blue balls) of Mn(dhbq)·2H_2O.

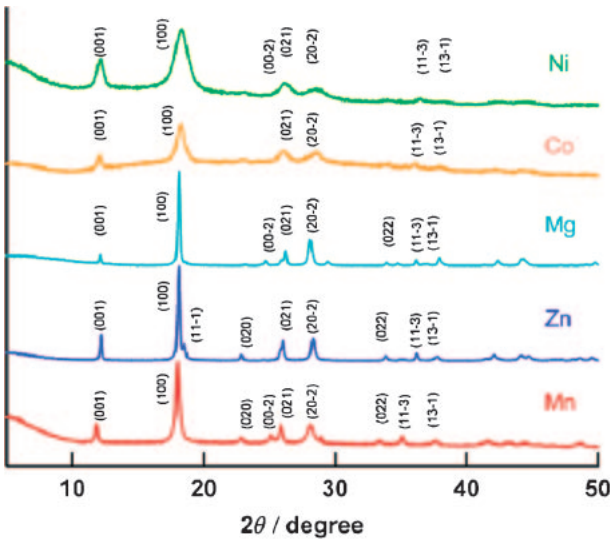

Figure 4. XRPD patterns of M(dhbq)·$n$$H_2O$ (λ = 1.0028 Å).

the void, and the differences in the EAs are thought to be derived from non-coordinating materials in the void.

Single crystals of metal–dhbq were not obtained by the diffusion method except for Mn compounds, and XRPD patterns of metal–dhbq compounds were collected as shown in Figure 4. The profiles for these CPs are in good agreement with those simulated from the crystal structure of Mn(dhbq)·2H_2O (Figure 3). Thus, these CPs are isostructural and form 1D structures, and are also thought to have vacancies for more adsorbent molecules. The peak widths depend on the metal species, indicating differences in crystal sizes. Ni compounds showed broad peak patterns, which were derived from large structural disorders.

Thermogravimetric Analysis. The water content of these compounds was evaluated by TG analysis, as shown in Figure 5. From the profiles, these CPs can be classified into three groups. Mn and Zn compounds lose two equivalents of water around 120 and 140 °C, respectively, while Co and Mg compounds lose a total of 2.5 equivalents of water below 180 °C. The Ni compound gradually loses weight below 100 °C and loses more up to 300 °C. The eliminated water content of these compounds estimated from TG analysis was in agreement with the values from EA. Because the water molecules contained in these dhbq compounds were eliminated at considerably higher temperature than boiling point, these water molecules must be tightly fixed with hydrogen bonds to the oxygen atoms of adjacent dhbq ligands, as well as to metal

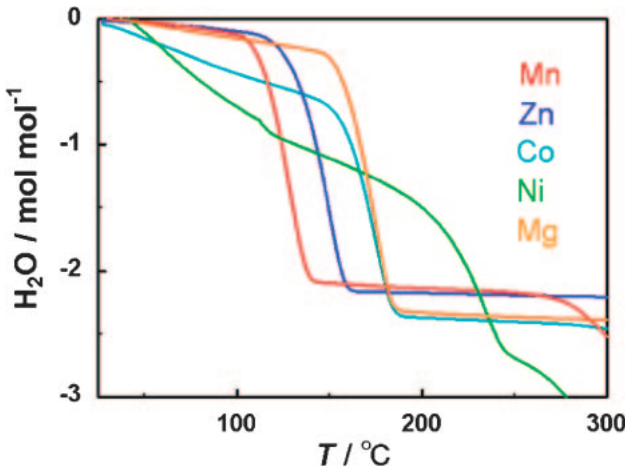

Figure 5. Thermal analysis data of M(dhbq)·nH$_2$O.

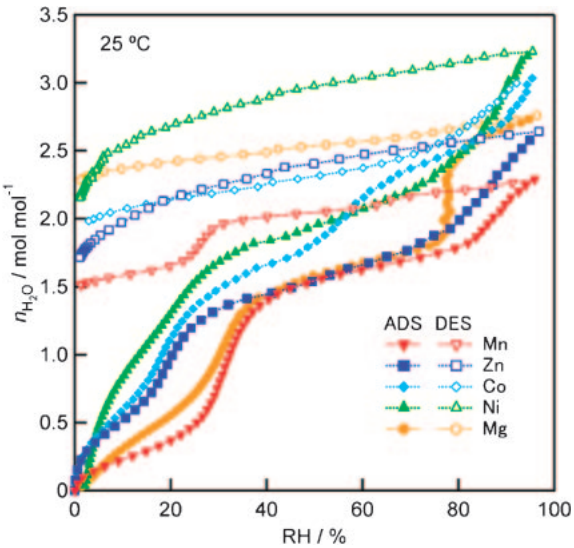

Figure 6. Water pressure–composition isotherms of M(dhbq) at 25 °C.

sites. In comparison between 3d metal ions, the stronger Lewis acidity of the metal site provides the higher water elimination temperature. Mg compound has similar lattice parameters to Zn compound, however water elimination temperature is higher. The Lewis acidity of Mg is weak, therefore the high elimination temperature is thought to be caused by the stronger hydrogen-bond networks. The Ni compound gradually loses almost one equivalent of water below 100 °C. The water-elimination behaviors of 1D metal oxalates were also evaluated, and nickel oxalate loses water at low temperatures, similarly to the dhbq compounds. Therefore, the gradual decrease in weight of the species is thought to be derived from weak coordination bonds from axial water molecules.

Water Absorption and Elimination Measurements. EA and TG measurements suggested that the Mg, Co, and Ni compounds contained more than two equivalents of water, however no difference was observed between the powder diffraction patterns of these compounds and the Mn and Zn compounds. To clarify the relationship between water content, metal species, and humidity conditions, pressure–composition isotherms (PCTs) of these compounds were measured (Figure 6). The specimens used for the PCT measurements were evacuated at elevated temperature before measurement, and were found to be totally dehydrated by measuring their weight loss.

As shown in the figure, stepwise absorption of water was observed at all profiles, and plateaus were observed at approximately 0.5 and 2.0 hydrated states for Mn(dhbq), 0.7 and 2.0 for Mg(dhbq), Co(dhbq), and Zn(dhbq), and 1.2 and 2.0 for Ni(dhbq). Excess hydration steps were observed at over 70% relative humidity (RH) for all compounds.

From these results, it was revealed that the dihydrate states of all compounds were stable at appropriate humidity conditions however other phases are also stable in other humidity ranges. In particular, all dhbq compounds have higher hydration states under greater than 80% RH.

The humidity dependence of XRPD patterns was also evaluated. Powder diffraction patterns of the fully evacuated state were changed drastically from those at ambient conditions. This suggests that stacking geometry and hydrogen-bonding arrangements are changed by elimination of coordinating water, because of the stabilizing coordination geometry of the metal ions. The crystal structure of anhydrated 1D iron(II) oxalate was reported to have a changed arrangement of the adjacent 1D iron(II) oxalate planes because of gaining coordination of an oxygen atom of an oxalate ligand to the metal site of the adjacent 1D metal oxalate chain. Crystal structures of M(dhbq)s are thought to be similar to the iron(II) oxalate anhydrate.

In contrast, the peaks of the diffraction patterns of these CPs do not shift with humidification. As described in the structure section, residual electron density peaks were observed in the crystal structure of Mn(dhbq)·2H$_2$O, therefore if more than two water molecules are absorbed, the additional water molecules are thought to occupy the void in the crystals of the M(dhbq)s. Therefore, absorbed water molecules at high humidity, which were seen as a bend at around 90% RH in Figure 6, do not expand the interchain distance or the chain pitch much. We have also measured the water uptake isotherms of 1D M(ox), which are isostructural to M(dhbq). The M(ox) has only a dihydrate state under high humidity. As dhbq is a longer ligand than oxalate, the above results suggest that dhbq provides voids in the CPs, and excess water molecules can be absorbed to those voids as zeolitic absorption. There are no reports concerning the hydrated and dehydrated states of metal dhbq compounds, and Mg(dhbq)·2.5H$_2$O, Co(dhbq)·2.5H$_2$O, and Ni(dhbq)·3H$_2$O are reported here for the first time.

X-ray Powder Pattern Refinement. Crystal structures of M(dhbq)·2H$_2$O were investigated using the Rietveld method. Details of the fitting method and refinement parameters are listed in the experimental section. Figure 7 shows the results of the refinements as well as comparisons of simulated and experimental patterns, and differences between them. Their lattice parameters are shown in Table 1. As shown in the figure, all XRPD patterns of M(dhbq)s can be fitted well to those simulated from isostructural Mn(dhbq)·2H$_2$O.

While the Co and Mg compounds were assumed to contain an excess of water molecules, as shown in Figure 8, the oxygen atoms of noncoordinating water molecules are located at almost the same positions as the voids that were observed as residual

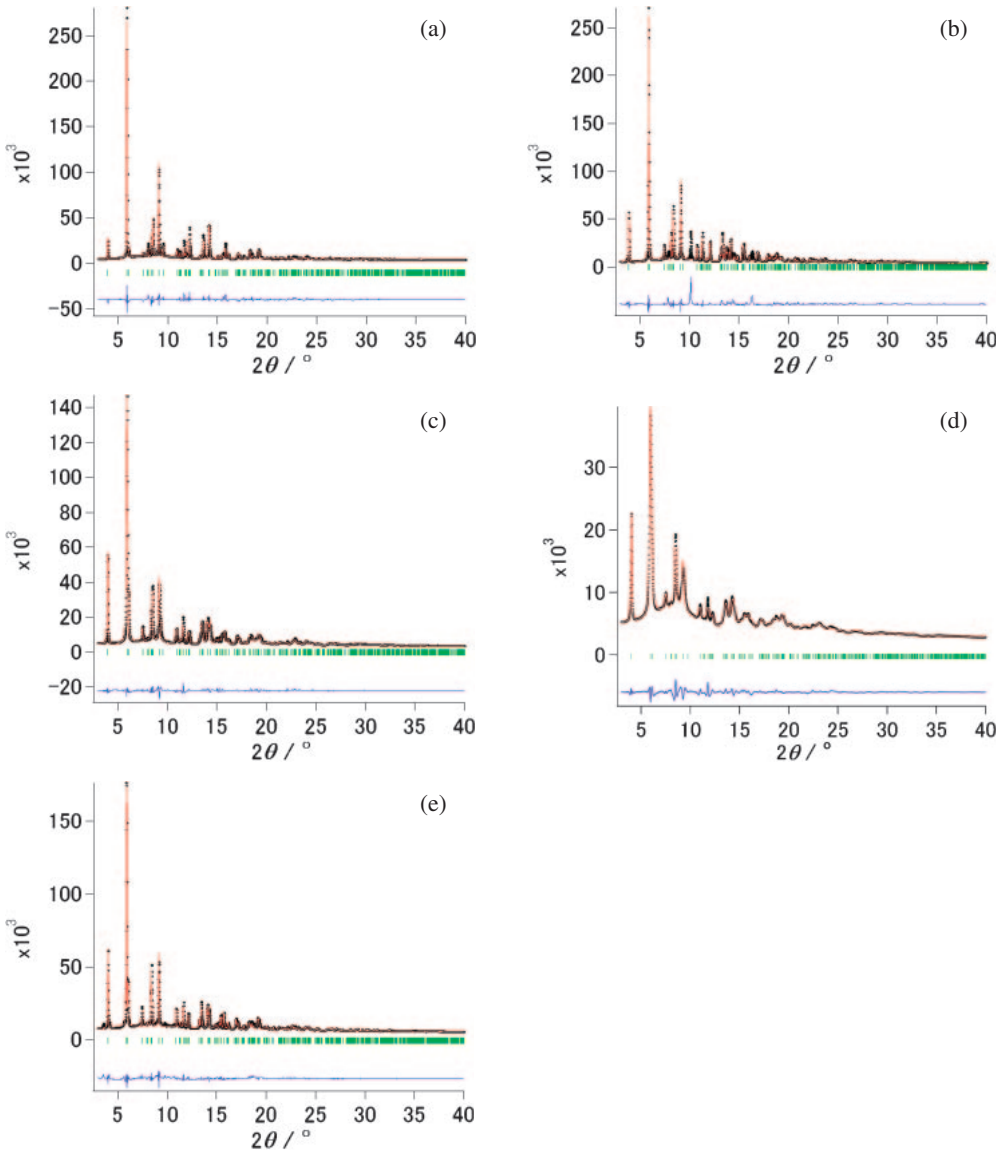

Figure 7. Result of Rietveld refinement of (a) Mg(dhbq)·2.5H_2O, (b) Mn(dhbq)·2H_2O, (c) Co(dhbq)·2.5H_2O, (d) Ni(dhbq)·3H_2O, and (e) Zn(dhbq)·2H_2O. Dotted, line, bars, and the line below the profiles represents experimental XRPD patterns of the sample, simulated patterns, observed reflection markers, and the differences between experimental and simulated value, respectively.

peaks of electron density in the crystal structure of the Mn compound (Figure 3).

Cell parameters of the Ni compound were estimated to be remarkably different from those of the other compounds. Peaks in the XRPD pattern for Ni are also found to be broad, indicating that the crystals are small and there is higher disorder in the crystal. By comparison with the other compounds, it can be observed that the length of the *c* axis is changed rather more than that of the *a* or *b* axis. The *c* axis represents the length of the 1D chain, therefore it is thought to be directly affected by the change in ionic radii.

Selected bond lengths estimated from the Rietveld refinements are listed in Table 2 and as shown in the table, the distances between metal sites and oxygen atoms of dhbq ligands depend on the metal species, and the differences are well correlated to the ionic radii of divalent octahedral metal ions in the literature.[15] On the other hand, the bond length between Mg and the oxygen atom (Mg–O(1)) of the coordinating water is similar to that of Mn–O(1), even though those of Co–O(1) and Zn–O(1) are shorter than Mn–O(1). Bond lengths of C(1)–C(1)′, C(1)–C(2), and C(1)–O(2) have smaller correlation to the metal size, indicating that the atomic coordinates of light elements have large errors, and precise analysis and computational study will provide the structural differences between them.

From the TG analysis, Mg and Co compounds contain a half equivalent of water at each metal site. From Rietveld refinement, the noncoordinating water was found in the void. Adsorbed water molecules make strong hydrogen bonds with coordinating water at an O···O distance of 2.71(10) Å, and a proton was presumably transferred from the coordinating water.

Proton Conductivity. Proton conductivities of dhbq compounds were evaluated using AC impedance. Figure 9 shows the proton conductivities of M(dhbq)·*n*H_2O at various

Table 1. Results of Rietveld Refinement of M(dhbq)·nH_2O Calculated with Powder Pattern Fitting

	Sample, M				
	Mg	Co	Mn	Zn	Ni
Water content (n)	2.5	2.5	2	2	3
Temperature/K	298	298	298	298	298
Wavelength/Å	0.502937	0.502937	0.502937	0.502937	0.502937
Fitted profile range	3–74°	3–74°	3–74°	3–74°	3–74°
2θ step increment	0.010	0.010	0.010	0.010	0.010
Space group	$C2/m$	$C2/m$	$C2/m$	$C2/m$	$C2/m$
Lattice parameters					
a/Å	6.8663(3)	6.8032(4)	6.9262(5)	6.8309(3)	6.6959(9)
b/Å	7.6687(3)	7.6806(4)	7.7418(5)	7.7450(3)	7.6783(13)
c/Å	7.8558(3)	7.8700(4)	8.0982(5)	7.8372(3)	7.7467(11)
β/°	112.483(5)	112.702(8)	113.890(7)	112.817(4)	111.919(17)
V/Å^3	382.21(6)	379.37(8)	397.03(10)	382.18(5)	369.5(2)
R_{wp}/%	6.35	3.80	10.59	4.15	2.67
R_p/%	4.10	2.44	5.45	2.53	1.76

Table 2. Selected Bond Lengths/Å of M(dhbq)·nH_2O

	Sample, M					
	Mg	Co	Mn	Zn	Ni	Mn[a)]
M–O(1)	2.247(10)	2.251(3)	2.174(14)	1.975(12)	2.090(10)	2.173(3)
M–O(2)	2.080(6)	2.159(4)	2.09(2)	1.966(11)	2.058(9)	2.168(2)
O(2)–C(1)	1.186(12)	1.233(5)	1.29(2)	1.430(18)	1.539(17)	1.263(4)
C(1)–C(1)′	1.610(14)	1.569(4)	1.533(18)	1.42(2)	1.36(2)	1.544(3)
C(1)–C(2)	1.540(12)	1.429(3)	1.437(19)	1.452(19)	1.433(17)	1.393(4)

a) Estimated from the crystallographic data reported elsewhere.[10]

humidities. DC conductivity of these specimens was very low, indicating that these compounds show low electronic conductivity. As discussed previously, protons do not conduct in anhydrous Mn(dhbq).[10] Proton conductivity depends both on the metal species and the RH. The proton conductivity of all samples increased with humidification, showing the effect of absorption of water in the 1D compound. The proton conductivity of Co(dhbq) increases with humidity but the change becomes moderate above 80% RH. As seen in the PCT measurement, the Co compound showed absorption of crystalline water from 40 to 80% RH to form the 2.5 hydrated state. On the other hand, the Mg and Zn compounds showed hydration from 40 to 100% RH and the 2.5 hydrated states were observed only at the fully humidified condition. The proton conductivity of these compounds showed a continuous increase with humidification to 100% RH. These results show that while metal–dhbq dihydrates do not show high conductivity, the conductivity increases remarkably when noncoordinating crystalline water is absorbed into the voids of the 1D array with humidity. From the crystal structure, a connected hydrogen-bond network seems to improve the proton diffusion in the direction of the 1D chain. The proton conductivity of Co(dhbq) is lower than that of Mn(dhbq) and Zn(dhbq) above 80% RH. The difference in conductivity could be related to the differences in Lewis acidity.

The Ni compound shows higher conductivity in the low humidity range of 40–90% RH. From EA, TG, and PCT measurements, Ni(dhbq) contains three water molecules at ambient humidity, and its higher disorder was shown by the XRPD measurements. Its high proton conductivity in lower humidity conditions is therefore also considered to result from the stacking disorder when it contains water molecules.

Proton conductivities of these compounds were much higher than those of bulk solids such as ice. The proton carriers of the M(dhbq)·nH_2O compounds are derived only from the water molecules, therefore carrier density seems to be increased by the electron-withdrawing effect of the Lewis acidic metal ions. In recent reports, heterogeneous impurities were reported to affect the proton conductivity critically by a doping of proton donor or acceptor sites at the interface of the media and the impurity.[5] Absorbed water molecules in the M(dhbq)s act as the impurity in these reports. This result also indicates that a connected proton conducting pathway also promotes the proton conductivity, even in the interfacial proton conduction. Site occupancy of noncoordinating water molecules in M(dhbq)s is small and the noncoordinating waters are thought to transport quickly. Therefore, the proton conduction mechanism of these compounds is mainly a vehicle mechanism in the high humidity region.[16]

Conclusion

To summarize, 1D CPs consisting of various metal ions and dhbq were synthesized and the structures of M(dhbq)·nH_2O were solved by the Rietveld refinement method. From EA, TG analysis, and PCT measurement, the metal–dhbqs showed reversible absorption and desorption of water molecules. The 2.5 hydrated states of Co and Zn compounds were identified by TG, EA, and PCT measurements, and the other compounds

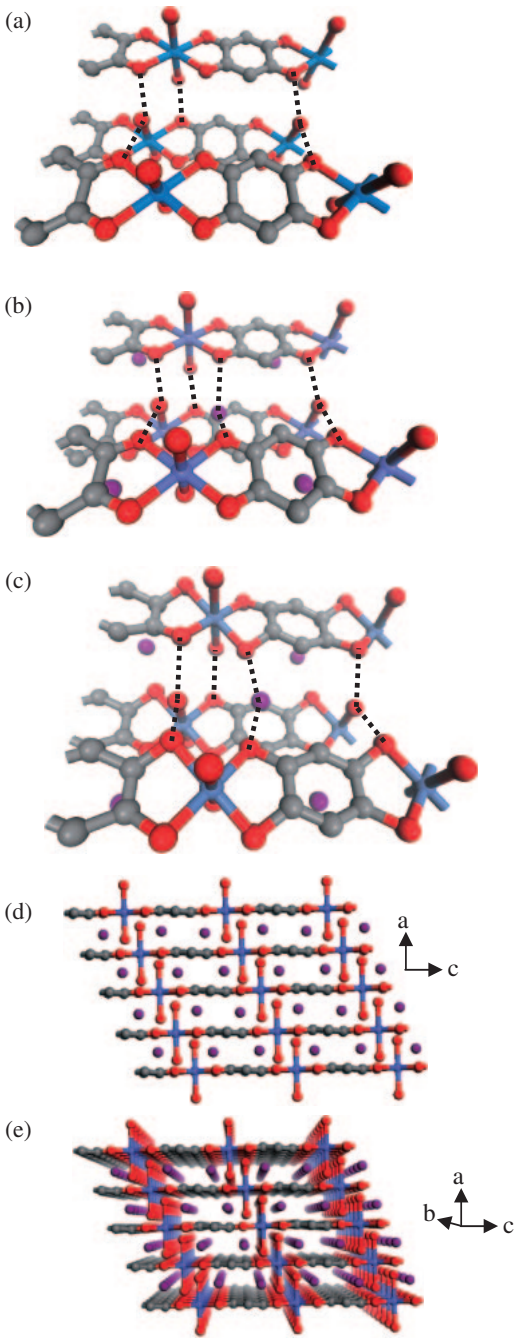

Figure 8. Crystal structures of (a) Mn(dhbq)·2H_2O, (b) Co(dhbq)·2.5H_2O, (c) Ni(dhbq)·3H_2O, (d) Co(dhbq)·2.5H_2O along the *ac* plane, and (e) perspective view of Co(dhbq)·2.5H_2O. Red: O; Blue: Mn, Co, or Ni; Gray: C. Dotted lines represent some of the hydrogen bonds. The purple sphere represents the half occupied (b) or fully occupied (c) oxygen atoms of noncoordinating water molecules.

also have the potential to absorb more than two water molecules. The proton conductivity of these compounds was 10^{-4} S cm^{-1} for Ni, Mg, Mn, and Zn compounds, while that for the Co compound was 10^{-5} S cm^{-1}. The proton conductivity of these compounds increased in the 2.5 hydrate states, and the mechanism was presumed to be a vehicle mechanism.

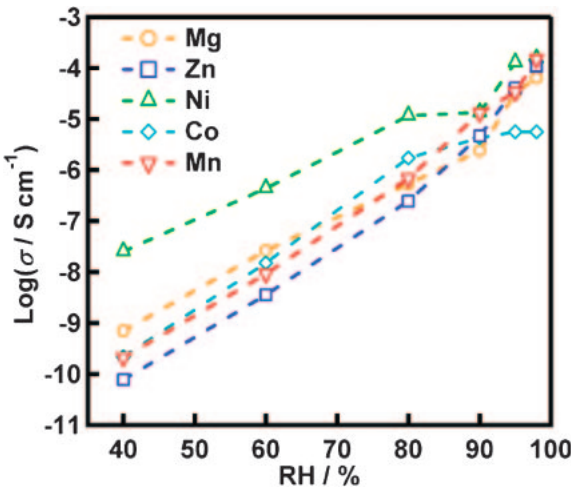

Figure 9. Proton conductivity of M(dhbq)·2H_2O at various humidities.

Experimental

General. Disodium 2,5-dioxido-1,4-benzoquinone (Na_2(dhbq)) was purchased from Wako Pure Chemical Industries, Ltd. Manganese sulfate pentahydrate ($MnSO_4$·5H_2O), cobalt sulfate heptahydrate ($CoSO_4$·7H_2O), nickel sulfate hexahydrate ($NiSO_4$·6H_2O), zinc sulfate heptahydrate ($ZnSO_4$·7H_2O), and magnesium sulfate heptahydrate ($MgSO_4$·7H_2O) were purchased from Kishida Reagents. All chemicals were used without further purification.

Details of Analyses. TG analysis was executed using a TG-DTA 2000SA (Bruker AXS). Specimens were put into aluminum dishes, and the measurements were conducted at a heating rate of 10 K min^{-1} under a nitrogen gas flow rate of 100 mL min^{-1}.

Water uptake measurement was performed using BELSORP 18 Plus (Bel Japan) at 25 °C. All samples used for conductivity measurements were heated to 50 °C under dynamic vacuum overnight. The samples were compressed to approximately 0.5 mm in thickness and 2.5 mm in diameter. Both sides of the pellets were attached to gold wires with gold paste. The specimens were exposed to a controlled temperature and humidity environment, and the conductivity measurements were carried out using a Solartron 1260 impedance/gain-phase analyzer by a quasi-four-probe method, and a 1296 dielectric interface and a two-probe method for the high-impedance range. A semicircle was observed in the Nyquist plot derived from Debye relaxation at each temperature and humidity condition, and the proton conductivity of these compounds was calculated from the diameter of the semicircle.

Synthesis Procedures. Synthesis of M(dhbq)·*n*H_2O: In a typical synthesis, a stirred solution of Na_2(dhbq) (184 mg, 1.0 mmol) in 20 mL of water was added to a solution of $MnSO_4$·5H_2O (241 mg, 1.0 mmol) in 50 mL of water. The precipitate was filtered off and dried, and Mn(dhbq)·2H_2O was obtained as a red powder. Yield: 331 mg (90.3%), Elemental analysis calculated (found) for $MnC_6H_6O_6$: C, 31.46% (31.06%); H, 2.64% (2.60%); Mn, 23.99% (23.77%). Results of the synthesis procedures are listed in Table 3.

Structural Analysis. High-resolution powder diffraction patterns of Mg(dhbq)·2.5H_2O, Mn(dhbq)·2H_2O, Co(dhbq)·2.5H_2O, Ni(dhbq)·3H_2O, and Zn(dhbq)·2H_2O were collected using a synchrotron radiation source at the BL02B2 beamline,

Table 3. Results of the Syntheses

	Sample, M				
	Mg	Mn	Co	Ni	Zn
Water content (n)	2.5	2	2.5	3.3	2
Color	pink	red	purple	purple	purple
Yield/%	81.3	90.3	7.51	87.0	93.9
Elemental analysis					
C_{calcd} (C_{found})/%	34.74 (34.70)	31.46 (31.06)	29.77 (29.78)	28.13 (27.97)	30.09 (29.96)
H_{calcd} (H_{found})/%	3.40 (3.24)	2.64 (2.60)	2.92 (2.90)	3.38 (3.02)	2.53 (2.59)
M_{calcd} (M_{found})/%	11.72 (11.58)	23.99 (23.77)	24.35 (24.35)	22.91 (23.20)	27.30 (26.37)

Spring-8 (Japan). The wavelength of the X-ray was determined from the XRPD pattern of a CeO_2 standard.

The structures of these compounds were first refined using Rietveld refinement.[17] Powder refinement was executed on Materials Studio (Accerlys). Pseudo-Voigt functions with five profile parameters were used for the refinements over 2θ ranges of 3.0–74.00° (with a step size of 0.010°). March–Dollase parameters were used for the refinement of preferred orientation.[18] The unit cell parameters and the 2θ zero-point shifts were refined. Twenty coefficients were used to describe the background. All the atomic coordinates were refined. The anisotropic temperature factor was used to refine the metal sites, while the isotropic temperature factor was used for the other light elements, and all were refined individually. Crystallographic data have been deposited with Cambridge Crystallographic Data Centre: Deposition numbers CCDC-752731 to -752735. Copies of the data can be obtained free of charge via http://www.ccdc.cam.ac.uk/conts/retrieving.html (or from the Cambridge Crystallographic Data Centre, 12, Union Road, Cambridge, CB2 1EZ, U.K.; Fax:+44 1223 336033; e-mail: deposit@ccdc.cam.ac.uk).

References

1 a) S. Kitagawa, M. Kondo, *Bull. Chem. Soc. Jpn.* **1998**, *71*, 1739. b) H. Li, M. Eddaoudi, M. O'Keeffe, O. M. Yaghi, *Nature* **1999**, *402*, 276. c) A. K. Cheetham, G. Férey, T. Loiseau, *Angew. Chem., Int. Ed.* **1999**, *38*, 3268. d) D. J. Tranchemontagne, J. L. Mendoza-Cortés, M. O'Keeffe, O. M. Yaghi, *Chem. Soc. Rev.* **2009**, *38*, 1257. e) O. Delgado-Friedrichs, M. O'Keeffe, O. M. Yaghi, *Phys. Chem. Chem. Phys.* **2007**, *9*, 1035.

2 a) L. Pan, D. H. Olson, L. R. Ciemnolonski, R. Heddy, J. Li, *Angew. Chem., Int. Ed.* **2006**, *45*, 616. b) B. Chen, C. Liang, J. Yang, D. S. Contreras, Y. L. Clancy, E. B. Lobkovsky, O. M. Yaghi, S. Dai, *Angew. Chem., Int. Ed.* **2006**, *45*, 1390. c) X. Lin, A. J. Blake, C. Wilson, X. Z. Sun, N. R. Champness, M. W. George, P. Hubberstey, R. Mokaya, M. Schröder, *J. Am. Chem. Soc.* **2006**, *128*, 10745.

3 a) K. Schlichte, T. Kratzke, S. Kaskel, *Microporous Mesoporous Mater.* **2004**, *73*, 81. b) T. Uemura, R. Kitaura, Y. Ohta, M. Nagaoka, S. Kitagawa, *Angew. Chem., Int. Ed.* **2006**, *45*, 4112. c) T. Uemura, Y. Ono, K. Kitagawa, S. Kitagawa, *Macromolecules* **2008**, *41*, 87. d) M. Alvaro, E. Carbonell, B. Ferrer, F. X. Llabrés, H. Garcia, *Chem.—Eur. J.* **2007**, *13*, 5106.

4 a) R. Kitaura, K. Seki, G. Akiyama, S. Kitagawa, *Angew. Chem., Int. Ed.* **2003**, *42*, 428. b) K. Uemura, S. Kitagawa, M. Kondo, K. Fukui, R. Kitaura, H.-C. Chang, T. Mizutani, *Chem.—Eur. J.* **2002**, *8*, 3586. c) S. Decurtins, H. W. Schmalle, H. R. Oswald, A. Linden, J. Ensling, P. Gütlich, A. Hauser, *Inorg. Chim. Acta* **1994**, *216*, 65. d) L. Pérez-García, D. B. Amabilino, *Chem. Soc. Rev.* **2007**, *36*, 941.

5 a) V. G. Ponomareva, G. V. Lavrova, L. G. Simonova, *Solid State Ionics* **1999**, *118*, 317. b) M. Tatsumisago, T. Tezuka, A. Hayashi, K. Tadanaga, *Solid State Ionics* **2005**, *176*, 2909. c) A. L. Despotuli, V. I. Nikolaichik, *Solid State Ionics* **1993**, *60*, 275.

6 a) J. Maier, *Nat. Mater.* **2005**, *4*, 805. b) S. Beyazyildirim, K. D. Kreuer, M. Schuster, A. J. Bhattacharyya, J. Maier, *Adv. Mater.* **2008**, *20*, 1274. c) N. Sata, K. Eberman, K. Eberl, J. Maier, *Nature* **2000**, *408*, 946. d) J. Maier, *Phys. Chem. Chem. Phys.* **2009**, *11*, 3011.

7 T. Yamada, H. Kitagawa, *J. Am. Chem. Soc.* **2009**, *131*, 6312.

8 a) H. Kitagawa, Y. Nagao, M. Fujishima, R. Ikeda, S. Kanda, *Inorg. Chem. Commun.* **2003**, *6*, 346. b) Y. Nagao, R. Ikeda, S. Kanda, Y. Kubozono, H. Kitagawa, *Mol. Cryst. Liq. Cryst.* **2002**, *379*, 89. c) Y. Nagao, R. Ikeda, K. Iijima, T. Kubo, K. Nakasuji, H. Kitagawa, *Synth. Met.* **2003**, *135–136*, 283. d) Y. Nagao, T. Kubo, K. Nakasuji, R. Ikeda, T. Kojima, H. Kitagawa, *Synth. Met.* **2005**, *154*, 89.

9 a) T. Yamada, M. Sadakiyo, H. Kitagawa, *J. Am. Chem. Soc.* **2009**, *131*, 3144. b) M. Sadakiyo, T. Yamada, H. Kitagawa, *J. Am. Chem. Soc.* **2009**, *131*, 9906.

10 a) H. Miyoshi, M. Matsumoto, S. Kanda, *J. Colloid Interface Sci.* **1997**, *193*, 26. b) H. Miyoshi, H. Mihara, S. Kanda, *Bull. Chem. Soc. Jpn.* **1996**, *69*, 1933.

11 R. S. Bottei, J. T. Fangman, *J. Inorg. Nucl. Chem.* **1966**, *28*, 1259.

12 A. M. Talati, V. N. Mistry, *Mater. Sci. Eng.* **1972**, *10*, 287.

13 a) T. R. Rao, P. R. Rao, P. Lingaiah, L. S. Deshmukh, *J. Indian Chem. Soc.* **1991**, *68*, 458. b) T. R. Rao, P. Lingaiah, L. Sirdeshmukh, S. Mehdi, *J. Indian Chem. Soc.* **1989**, *66*, 826. c) T. R. Rao, P. Lingaiah, L. Sirdeshmukh, *J. Indian Chem. Soc.* **1990**, *67*, 832.

14 S. Morikawa, T. Yamada, H. Kitagawa, *Chem. Lett.* **2009**, *38*, 654.

15 R. D. Shannon, *Acta Crystallogr., Sect A* **1976**, *32*, 751.

16 a) Ph. Colomban, A. Novak, *J. Mol. Struct.* **1988**, *177*, 277. b) K. D. Kreuer, *J. Membr. Sci.* **2001**, *185*, 29.

17 H. M. Rietveld, *Acta Crystallogr.* **1967**, *22*, 151.

18 W. A. Dollase, *J. Appl. Cryst.* **1986**, *19*, 267.